

HOSTED BY



Contents lists available at ScienceDirect

Saudi Pharmaceutical Journal

journal homepage: www.sciencedirect.com



Original article

Draft genome sequence of potato crop bacterial isolates and nanoparticles-intervention for the induction of secondary metabolites biosynthesis

Nada Al-Theyab^{a,b}, Omar Alrasheed^b, Hatem A. Abuelizz^{b,*}, Mingtao Liang^{a,*}

^a School of Biomedical Science and Pharmacy, University of Newcastle, Callaghan, New South Wales, Australia

^b Department of Pharmaceutical Chemistry, College of Pharmacy, King Saud University, Riyadh 11451, Saudi Arabia



ARTICLE INFO

Article history:

Received 27 February 2023

Accepted 17 April 2023

Available online 23 April 2023

Keywords:

Potato crops

Genomics

Priestia megaterium

Biosynthetic gene clusters

Secondary metabolite

Gold nanoparticle

ABSTRACT

Introduction: Insights about the effects of gold nanoparticles (AuNPs) on the biosynthetic manipulation of unknown microbe secondary metabolites could be a promising technique for prospective research on nano-biotechnology.

Aim: In this research, we aimed to isolate a fresh, non-domesticated unknown bacterium strain from a common scab of potato crop located in Saudi Arabia and study the metabolic profile.

Methodology: This was achieved through genomic DNA (gDNA) sequencing using Oxford Nanopore Technology. The genomic data were subjected to several bioinformatics tools, including canu-1.9 software, Prokka, DFAST, Geneious Prime, and AntiSMASH. We exposed the culture of the bacterial isolate with different concentrations of AuNPs and investigated the effects of AuNPs on secondary metabolites biosynthesis using several analytical techniques. Furthermore, Tandem-mass spectrometric (MS/MS) technique was optimized for the characterization of several significant sub-classes.

Results: The genomic draft sequence assembly, alignment, and annotation have verified the bacterial isolate as *Priestia megaterium*. This bacterium has secondary metabolites related to different biosynthetic gene clusters. AuNPs intervention showed an increase in the production of compounds with the molecular weights of 254 and 270 Da in a direct-dependent manner with the increase of the AuNPs concentrations.

Conclusion: The increase in the yields of compound 1 and 2 concomitantly with the increase in the concentration of the added AuNPs provide evidences about the effects of nanoparticles on the biosynthesis of the secondary metabolites. It contributes to the discovery of genes involved in different biosynthetic gene clusters (BGCs) and prediction of the structures of the natural products.

© 2023 The Author(s). Published by Elsevier B.V. on behalf of King Saud University. This is an open access article under the CC BY-NC-ND license (<http://creativecommons.org/licenses/by-nc-nd/4.0/>).

1. Introduction

Microbes are capable of producing a myriad number of secondary metabolites that hold great potential for drug development (Antoraz et al., 2015). The production of secondary metabolites has

generally been carried out using in-vitro microbial cultures. However, due to employment of conventional cultivation conditions, there is a high rate of redundancy that results in the frequent isolation of already known compounds rather than discovery of novel compounds (Antoraz et al., 2015). Apparently, microbes have an extensive range of gene clusters coding for secondary metabolites in which only some are transcribed in experimental conditions and the others remain silent and are not expressed (Wang et al., 2019). In the past years, great progress has been made in characterizing the biosynthetic gene clusters (BGCs) responsible for the main categories of secondary metabolites such as alkaloids, isoprenoids, and phenylpropanoids (Kumar et al., 2018). Genetic engineering approaches have been developed to manipulate BGC expression to enhance the production of known secondary metabolites or produce new natural products. However, the genetic engineering

* Corresponding authors.

E-mail addresses: habuelizz@ksu.edu.sa (H.A. Abuelizz), roger.liang@newcastle.edu.au (M. Liang).

Peer review under responsibility of King Saud University. Production and hosting by Elsevier.



Production and hosting by Elsevier

<https://doi.org/10.1016/j.jsps.2023.04.016>

1319-0164/© 2023 The Author(s). Published by Elsevier B.V. on behalf of King Saud University.

This is an open access article under the CC BY-NC-ND license (<http://creativecommons.org/licenses/by-nc-nd/4.0/>).

approaches are time-consuming and often require multiple cloning experiments and culture generations to achieve a suitable strain (Wang et al., 2019). Physical and chemical alterations of growth media have been routinely used to modulate the production of secondary metabolites in in-vitro cultures. These alterations can involve a change in the composition of growth media or growth conditions (e.g. pH, temperature, oxygenation), co-cultivation with competitors, or addition of precursors. For instance, changing the medium properties of microbial culture may increase the concentration of carbon and/ or nitrogen sources and influence the pH, which affects the metabolite production (Ruiz et al., 2010, Brzonkalik et al., 2012). Chemical elicitors can also be used to induce biotic or abiotic stress and activate certain BGCs otherwise remaining silent under laboratory culture conditions, which in turn results in the production of higher amounts or a new secondary metabolite (Zong et al., 2021). Metal ions are an example of an abiotic elicitor that has been demonstrated to activate silent BGCs and create unique secondary metabolites in different strains of *Streptomyces* (Zong et al., 2021). Early study postulated the potential application of nanoparticles (NPs) as a novel elicitor for secondary metabolites production due to their unique properties. There is ample evidence showing that NPs significantly impact the growth, development and physiology of plants and demonstrate elicitor activities for the enhancement of the secondary metabolites biosynthesis (Marslin et al., 2017, Mandal and Basu 2021). However, the focus on characterizing plant metabolism may be obscured due to the complex, multifactorial nature of diverse plant-associated bacteria that can interact with each other and their host through the actions of secreted metabolites (Mandal and Basu 2021). Over the past few decades, there has been great interest shown in the use of microorganisms for the synthesis of nanomaterials, e.g. selenium, gold, and silver NPs (Grasso et al., 2019). For example, *Bacillus* spp., including *B. subtilis*, *B. marisflavi*, and *B. licheniformis* have been utilized for the green biosynthesis of AuNPs (Singh et al., 2014, Srinath et al., 2018, Nadaf and Kanase 2019). On the other hand, emerging evidence shows that NPs can significantly impact the growth of microbes and that they have elicitor activities for the enhancement of secondary metabolite biosynthesis (Liu et al., 2019). There have been only a few reports of the NPs effect on microorganisms' growth characteristics and secondary metabolite profiles. Liu et al. studied the antibiotic production of *S. coelicolor* M145 in the presence of copper oxide (CuO) NPs. They found that low concentration of CuONPs increased the production of actinorhodin (ACT) antibiotics, whereas high concentrations inhibited this process (Liu et al., 2019). Common scab disease occurs throughout the world's potato-cultivating regions as an accusative agent of *Streptomyces scabies* and other strains, including *S. acidiscabies*, *S. turgidiscabies*, *S. ipomoeae*, and *S. griseoplanus* (Loria et al., 2006, Lambert et al., 2007, Cui et al., 2021). Numerous potato crops contain *Bacillus*, and they are known for their potential as biocontrol agents (Han et al., 2005, Khedher et al., 2015, Cui et al., 2021). *B. megaterium* L2 has yielded five bioactive compounds with antimicrobial activity: phenylacetic acid, behenic acid, erucamide, palmitic acid, and β -sitosterol (Xie et al., 2021). *B. megaterium* was reclassified into a proposed genus called *Priestia* in 2020 (Gupta et al., 2020); it was given the new official taxonomic name, *P. megaterium*. Biotechnological uses of *P. megaterium* have ranged from the manufacture of small molecules to polymers (Biedendieck et al., 2021). A recent study reported that *P. megaterium* DSM 509 is a potential source of polyhydroxyalkanoate polymers (Shahid et al., 2013, Alkotaini et al., 2015, Coltin et al., 2022).

The computational prediction of BGCs in genomics can lead to faster profiling of the bacterial metabolic potential (Blin et al., 2019). Several steps in genome mining should be considered, such as assembly and annotation of the whole genome sequence,

identification of BGCs, prediction of the structures of natural products, and comparative genomic analysis to determine similarities and differences across organisms. However, the quality of genome assembly and annotation of the sequence has a major impact on genome-based analysis (van Der Hooft et al., 2020). For instance, the assembly of a whole genome sequence contains many small 'fragmented' contigs. BGCs are likely to be fragmented among contigs. Therefore, it is especially difficult to collect entirely continuous BGC sequences from metagenome data. Some of the gene cluster fragments are often found on contigs that are shorter than the limit of detection by BGC identification techniques (van Der Hooft et al., 2020). Misassemblies are quite common, particularly during the assembly of genomes using short-read data with poor coverage. This might result in the skipping or "repetition" of non-ribosomal peptides (NRPs) or polyketide (PK) modules within a BGC (van Der Hooft et al., 2020). New developments in DNA sequencing technology and bioinformatics have enabled the mining of vast amounts of sequence data found in the genome and metagenome (Kenshole et al., 2021). Genome-mining tools such as AntiSMASH can be used to simplify BGC identification and compare unknown and known BGCs to generate highly accurate prediction informatics for secondary metabolomes (Blin et al., 2019).

The object of this research was to study the effect of AuNPs intervention on bacterial isolate culture to study their intervention on the secondary metabolites biosynthesis. Various concentrations of AuNPs were used during the culture period, and the effects of secondary metabolites production of the bacterial isolate upon addition of AuNPs were evaluated and validated using a variety of analytical methods.

2. Materials and methods

2.1. Materials

Tri-sodium citrate dihydrate was purchased from VWR Chemicals. All other chemicals were purchased from Sigma Aldrich, USA. Silicone oil was purchased from Acros Organics, N.V. Bacterial culture media was purchased from Watin-Biolife, Saudi Arabia.

2.2. Isolation, purification, characterization, and sequencing of whole gDNA of potato crop isolate

Potatoes from a supermarket in Riyadh were washed, peeled, surface sterilized with 96 % ethanol, and flamed according to the plant tissue isolation method (Suhandono et al., 2016). A piece of potato scab was aseptically cut. Thereafter, it is streaked onto a nutrient agar medium containing 0.4% (w/v) glucose, 0.4% (w/v) yeast extract, 1% (w/v) malt extract, and 2% (w/v) agar in distilled water and autoclaved. The mixture was poured into plates to make solid agar. The colonies appeared in three days, the bacterium strain was harvested and subcultured four times for further purification. The microbes were finally suspended in 40% (v/v) glycerol and stored at -80°C (Hoornstra et al., 2013). The Gram stain reaction was performed using a purified colony of the bacterium: rod-shaped Gram-positive cells were observed using Gram stain slides analyzed under an Olympus CH20BIMF200 compound bright-field microscope with 1,000x magnification (Sandle 2004). The whole gDNA of the isolate was extracted with the QIAamp DNA mini kit (Qiagen, Hilden, Germany) and prepared for sequencing on the Oxford Nanopore MinION sequencer using the ligation sequencing SQK-LSK109 kit according to the manufacturer's instructions (Oxford Nanopore Technologies, United Kingdom).

2.3. Assembly, identification, general characteristics, and phylogeny of the genomic draft

Reads were assembled into contigs using canu-1.9 software (Koren et al., 2017). Rapid genome annotation was performed using Prokka (Seemann 2014), and the resulting annotations. Whole genome alignments were performed using Geneious Prime (<https://www.geneious.com>). DFAST is a flexible prokaryotic genome annotation pipeline that effectively operates with default parameters when applied to well-characterized species like Actinobacteria, Firmicutes, and Proteobacteria (Tanizawa et al., 2017). The Circular Genome Viewer (CGView) is a Java program and library that generates zoomable, high-quality maps of circular genomes (Stothard and Wishart 2005). Geneious Prime is a software application that includes fundamental molecular biology and sequence analysis tools such as alignment, annotation, BLAST, tree building, and so on. Consequently, a phylogenetic tree of the strains was formed based on a BLAST search of the housekeeping gene from a bacterial isolate. Related strains with identical sites were compared.

2.4. Genome mining techniques for secondary metabolites identification

BGCs clusters were identified using bioinformatic tools for genome mining (Ren et al., 2020). For instance, AntiSMASH is a comprehensive tool for identifying a broad range of secondary metabolite BGCs in the bacterial genome (such as *Bacillus* sp.) to predict partial or whole BGCs clusters. The putative genes were compared with other known strains that have common BGCs clusters using the AntiSMASH tool (Pinjari and Bramhachari 2018). In addition, AntiSMASH is coupled with the Minimum Information about a Biosynthetic Gene cluster (MiBIG) database to develop a community standard for annotations and data on BGC detection and small molecule structure identification (Kautsar et al., 2020).

2.5. Synthesis and characterization of AuNPs

AuNPs were synthesized by aqueous reduction of tetrachloroauric acid (HAuCl₄) in the presence of trisodium citrate (Liang et al., 2010). Before AuNPs synthesis, all glassware was washed with appropriate amounts of aqua-regia; HCl/HNO₃ (v/v), 3:1 ratio, then rinsed several times with MilliQ water and oven-dried overnight. Briefly, to make 10 nm citrate-AuNPs, a total of 100 mL of MilliQ water and 7 mL of 1% sodium citrate solution were boiled together on a silicon oil bath then 1 mL of 1% HAuCl₄ solution was rapidly added. The reaction was stopped when the solution changed to a wine red colour. The particle size and size distribution of AuNPs were measured using dynamic light scattering (DLS, Zetasizer nano, Malvern Instruments Ltd.). Transmission electron microscopy (TEM) was used to characterize the morphology and size distribution of AuNPs, where the sample was viewed under JEM1010 transmission electron microscope (JEOL, Japan) at an operating voltage of 80 kV. The concentration of AuNPs was measured using ultraviolet–visible (UV–VIS) Spectrometer (Libra S22, Biochrom Ltd, England) and the concentration (c) was quantified using Beer-Lambert law, where the absorbance (A) of AuNPs solutions at a certain wavelength (nm) is directly related to the concentration of the solute in the solution, giving the following equation: **Absorbance(A)** = *exbc*. The extension coefficient (e) of 10 nm AuNP is $1.12 \times 10^8 \text{ cm}^{-1} \text{ M}^{-1}$ (Maye et al., 2003), and the path length (b) is 1 cm (Maye et al., 2003).

2.6. Bacterial culture with AuNPs intervention and extraction of crude metabolites

The bacterial isolate was cultured for 72 h on an agar plate containing the specified nutrients. Then, single colony of the grown

bacteria was inoculated into a 500 mL Erlenmeyer flask containing 300 mL of sterilized seed media [Glucose 0.4% (w/v), Yeast extract 0.4% (w/v), and Malt extract 1 % (w/v)] at a pH of 7.4, and the flask was incubated on an orbital shaker at 200 rpm for 72 h. The bacteria were further cultivated in the production media, which contained 10% (v/v) of seed media; 2 mL of the seed culture was added into 20 mL of tryptone soy broth (TSB) and co-cultured with various concentrations of AuNPs (0, 25, 50, 250, 500, 1000, 1500, and 2000 pM) at 30 °C in an orbital shaker incubator at 200 rpm. After six days of bacteria growth, the biomass was processed and harvested as previously reported (Kai 2020) for further extraction. To extract the crude secondary metabolites, the harvested biomass of bacteria growth was centrifuged for 15 min, at 5000 rpm and 5 °C to obtain cell-free supernatants. The cell-free supernatants were extracted with an equal volume of ethyl acetate. The organic layer was collected then evaporated by a rotary evaporator to obtain the crude metabolites. Finally, The dried sample was weighed and dissolved in methanol (MeOH) HPLC grade, filtered through 0.2 µm polyethersulphone (PES) syringe filters, and kept in the refrigerator until when needed (Xie et al., 2021).

2.7. LC-MS/MS analysis

The chromatographic analysis was performed on HPLC using the 2998 Waters® photodiode array (PDA) detector and 1525 Waters® binary HPLC pump. Separation processes were carried out (each for triplicate) on a reverse-phase C₈ column (150 mm × 4.6 mm, 5 µm) kept at 25 °C. Mobile phase: 0.1% (v/v) formic acid/ HPLC water (solvent A); 0.1% (v/v) formic acid/ MeOH (solvent B); flow rate 0.4 mL/min; injection volume: 10 µL. The gradient elution was carried out as follows solvent (B) 35–90% for 7 min, 90–90% for 7–25 min, 90–35% for 25–35 min. The absorbance spectrum scan was recorded between 210 and 400 nm to determine λ_{max} of the unknown compounds. Detection in the UV range was fixed at 280 nm. Compound identification by mass spectrometry was carried out using an Agilent 1200 HPLC that consists of G1367B HIP-ALS autosampler, G1322A degasser, G1316 thermostated column compartment and G1311A binary pump that was connected to an Agilent 6320 ion-trap (Agilent Technologies, Palo Alto, CA, USA) with an Agilent 6410 Triple Quadrupole ESI ion source. Mass Hunter software (Agilent Technologies, Palo Alto, CA, USA) was used to regulate the data acquisition and instruments. The injection was done using connector instead of column. The aqueous part of the mobile phase is 0.1% formic acid/ water (pH 3.2) at 0.2 mL/min flow rate. The organic part of the mobile phase is MeCN contains 0.1% formic acid. The injection volume of the sample was 5 µL with a total run time of 4 min. Mass scan mode was used for the detection of the compound ion peak. ESI operated in the positive charge ionization mode was utilized for ion generation. Nitrogen gas at a flow rate of 10 L/ min (generated by nitrogen generator) was used for spray drying in the ESI source collision (Abdelhameed et al., 2020). The product ions for the target compounds were formed inside the collision cell by collision induced dissociation (CID) 30 eV using helium gas as a collision gas. ESI operated in the positive charge ionization mode for ion generation. Flow injection analysis was used to mass spectrometric parameters optimization to attain the highest ion intensity. The values of ESI voltage and capillary temperature were adjusted at 4.5 kV and 325 °C, respectively. Characterization of compound fragments was performed using fragmentation mode for the mass transitions (parent to product ions) as Fragmentor voltage: 145 V and amplitude: 1.25 V (Abdelhameed et al., 2020).

3. Results and discussion

3.1. Characterization, morphology, and taxonomy of genomic draft bacterial isolate

Bacillus is a genus of widespread, rod-shaped bacteria that may be classed as Gram-positive, Gram-variable, aerobic, or facultatively anaerobic. *Bacillus* may adapt to a wide range of environmental conditions due to the ability to create endospores (Moat et al., 2002, Fekete 2005).

A single bacterial isolate was grown from a potato scab of a commercial potato on nutrient agar. The bacterium had circular, creamy, white dried colonies with rough edges. The isolate was a Gram-positive rod according to Gram-stain microscopy and is potentially from the *Bacillus* genus. *Bacillus* spp. potentially produces bioactive secondary metabolites; therefore, the strain was examined by genomic sequencing for use as a model.

3.2. Bacterial identification and general genome statistics

NCBI BLAST of a housekeeping gene (*gyrB*) was performed using (nr_nt) Megablast extracted from contig tig000000031 and the closest identity was *Priestia megaterium* (Table 1).

Phylogenetic analysis of the *gyrB* gene sequence revealed that our bacterial isolate contained a partial *gyrB* gene sequence that exhibited 100% similarity with *P. megaterium* strain BRIP 64817 (accession # MW057935). It fell into the same clade following nucleotide alignment consensus of *gyrB* sequences and phylogenetic analysis using Geneious prime software to construct a neighbor joining tree comparing seven different *Priestia* strains (Fig. 1). The taxonomy of the bacterial isolate belongs to Bacteria; Firmicutes; Bacilli; Bacillales; *Bacillaceae*; and *Priestia* using Geneious.

Average nucleotide identity (ANI) analysis was performed to confirm this result. Our genomic draft presents a high (ANI > 98%) cut-off value for defining bacteria belonging to the same species in the genomes of *P. megaterium*. The identified strain

Table 1
BLAST analysis of the *gyrB* gene from the bacterial isolate and % identical sites of related strains using Geneious software.

Organism	Strains	Accession number	% Identity
<i>Priestia megaterium</i> strain BRIP 64818 DNA gyrase subunit B (<i>gyrB</i>) gene, partial cds	BRIP 64,818	MW057936	99.7%
<i>Priestia megaterium</i> strain BRIP 64817 DNA gyrase subunit B (<i>gyrB</i>) gene, partial cds	BRIP 64,817	MW057935	99.4%
<i>Priestia megaterium</i> strain BP01R2 chromosome, complete genome	BP01R2	CP092387	99.4%
<i>Priestia megaterium</i> strain CDC 2008724142 chromosome, complete genome	CDC 2,008,724,142	CP069606	99.4%
<i>Priestia megaterium</i> strain 2020WEIHUA_L chromosome, complete genome	2020WEIHUA_L	CP059457	99.4%
<i>Priestia megaterium</i> strain FDU301 chromosome, complete genome	FDU301	CP045272	99.4%
<i>Priestia megaterium</i> NCT-2 chromosome, complete genome	NCT-2	CP032527	99.4%
<i>Priestia megaterium</i> strain ATCC 14581 chromosome, complete genome	ATCC 14,581	CP069288	99.3%
<i>Priestia megaterium</i> NBRC 15308 = ATCC 14581 chromosome, complete genome	ATCC 14,581	CP035094	99.3%
<i>Bacillus megaterium</i> NBRC 15308 = ATCC 14581, complete genome	ATCC 14,581	CP009920	99.3%
<i>Bacillus megaterium</i> DSM319, complete genome	DSM 319	CP001982	99.3%
<i>Bacillus megaterium</i> strain 899 DNA gyrase subunit B (<i>gyrB</i>) gene, partial cds	899	JN575334	99.0%

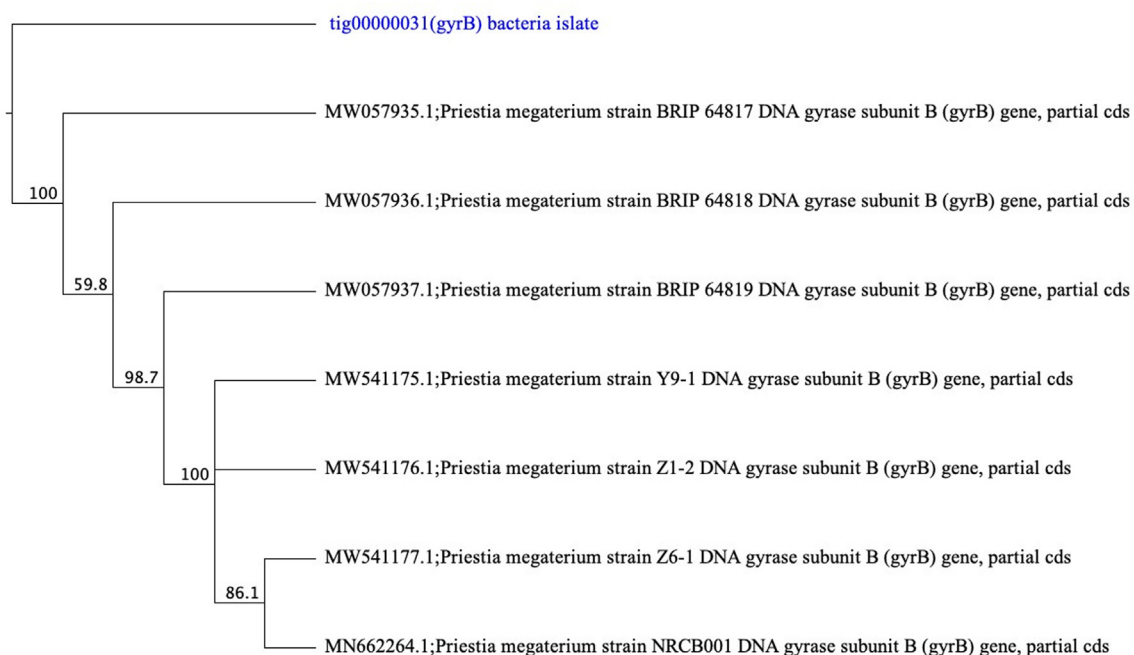


Fig. 1. Phylogenetic tree of *Priestia* strains constructed based on the *gyrB* gene sequence. Bootstrap values (%) presented at the branches were calculated from 1,000 replications using Geneious version 2023.0 created by Biomatters. Available from <https://www.geneious.com>.

Table 2

DFAST quality control of the genomic draft. The organism name inferred from the ANI result is *P. megaterium* based on NCBI assembly taken from the DFAST website: <https://dfast.ddbj.nig.ac.jp/analysis/annotation/d03a4b5f-5d70-4f4f-9595-4757552fe77>.

Organism	Strain	Accession	ANI%	Matched fragments	Total ragments
<i>Priestia megaterium</i>	ATCC 14,581	GCA_900113355.1	98.0407	1706	2226
<i>Priestia megaterium</i>	NBRC 15,308	GCA_001591525.1	97.4039	1610	2226
<i>Priestia megaterium</i>	ATCC 14,581	GCA_017086525.1	97.3839	1646	2226
<i>Priestia megaterium</i>	NCTC10342	GCA_900445485.1	97.3637	1641	2226
<i>Priestia megaterium</i>	ATCC 14,581	GCA_000832985.1	97.303	1653	2226
<i>Priestia megaterium</i>	ATCC 14,581	GCA_006094495.1	97.2912	1653	2226
<i>Bacillus tequilensis</i>	NCTC13306	GCA_900445435.1	80.7	55	2226
<i>Metabacillus iocasae</i>	DSM 104,297	GCA_016909075.1	78.499	269	2226
<i>Priestia filamentosa</i>	SGD-14	GCA_900177535.1	77.5834	252	2226
<i>Priestia filamentosa</i>	DSM 27,955	GCA_002237735.1	77.5745	251	2226
<i>Neobacillus thermocopriae</i>	SgZ-7	GCA_010975035.1	77.1423	74	2226
<i>Neobacillus sedimentimangrovi</i>	FJAT-2464	GCA_010614825.1	77.1044	74	2226
<i>Neobacillus cucumis</i>	DSM 101,566	GCA_016908975.1	77.0689	131	2226
<i>Alkalihalobacterium elongatum</i>	MEB199	GCA_019024285.1	76.2909	84	2226

(ATCC14581, accession # GCA_900113355.1) was predicted by DFAST analysis based on the NCBI assembly report and ANI report (Tables 2) and (Table 2a in supporting data file). The sequence contained 150 contigs, and a total length of 6,914,202 base pairs (bp). The average percentage of guanine-cytosine base pairs (GC%) was 37.5%. The number of rRNAs and tRNAs was 41 and 181, respectively. The total number of coding sequences (CDSs) was 11,822.

The circles in Fig. 2 represented the following description from outside to inside: the (G + C) content is represented in black, the (G + C) skew positive is in green, and the (G + C) skew negative is in purple. This map generates a visually characteristic graphical map of the bacterial genomic draft.

3.3. Bioinformatics analysis of the genomic draft and prediction of BGCs, together with secondary metabolites

Bioinformatic tools such as AntiSMASH enable rapid and automatic identification of the BGCs in bacterial genome sequences. The recently launched MIBiG repository provides rich reference data to connect the gene cluster families (GCFs) to their known products based on gene cluster homology, even across bacterial

genera. These tools were used to present a thorough review of the variety of BGCs with known products and uncharacterized chemicals in *P. megaterium* whole genome sequences across known BGCs. The genomic draft contains a sequence in the FASTA file of 150 contigs that were submitted to the AntiSMASH database. Seven identified putative secondary metabolites found using the AntiSMASH program (version 6.1.1) were related to the identified BGCs. The identified BGCs contained homology to *P. megaterium* based on several known biosynthetic classes of selected regions, and each region was related to a specific cluster (Fig. 3). The seven selected regions from the AntiSMASH database had the most similar known clusters and shared the same gene of known metabolites. Two regions (11.1 and 92.1) had known clusters, but no secondary metabolites were identified. The tig00000007 had two regions (regions 2.1 and 2.2) with unique gene clusters. Region 2.1 contained a hybrid PKS + NRPS cluster, while region 2.2 had a conserved NRPS BGC. Moreover, tig00000037 was located at region 11.1 and contained a T3PKS cluster. The most occupied region (tig00000069) was related to the transAT-PKS cluster. In addition, tig00004539 had two regions that contained terpene and NRP clusters: 89.1 and 89.2, respectively. The last region-identified cluster (92.1) showed an RiPP-like cluster. However, no BGCs were identified in most regions of the other 145 contigs.

In order to screen those secondary metabolites of the predictable BGCs, the AntiSMASH analysis suggested a genomic draft of *P. megaterium* that possesses seven BGCs, including two hybrid (PKS + NRPS), one class of T3PKS, one terpene, and two NRP and one RiPP-like. Bacillaene and carotenoid secondary metabolites exhibited moderate homology (40–80%). The remaining identified secondary metabolites (locillomycin, phosphinothricintripeptide, and ficellomycin) had low homologies (<40%) (Table 3).

P. megaterium is a widely studied model gram-positive bacterium; however, little is known about its secondary metabolites.

3.4. Characterization of AuNPs

AuNPs were formed by aqueous reduction of tetrachloroauric acid (HAuCl₄) in the presence of sodium citrate as previously reported (Liang et al., 2010). The DLS results show that the particle size of AuNPs particles was 9.7 nm ± 0.024 with a narrow PDI of 0.093 ± 0.018 (Fig. 4a). The DLS results are in agreement with TEM morphology analysis that indicated the formation of monodispersed spherical AuNPs with a mean size of ~ 10 nm and uniform distribution (Fig. 4b). Zeta potential was measured to be around – 20 mV owing to the presence of citrate stabilizer on the surface of AuNPs. The UV–VIS spectrum of the prepared AuNPs solution displayed a single absorption peak at 520 nm with an absorbance of 0.947 (Fig. 4c). According to Beer-Lambert law ($A = e * b * c$),

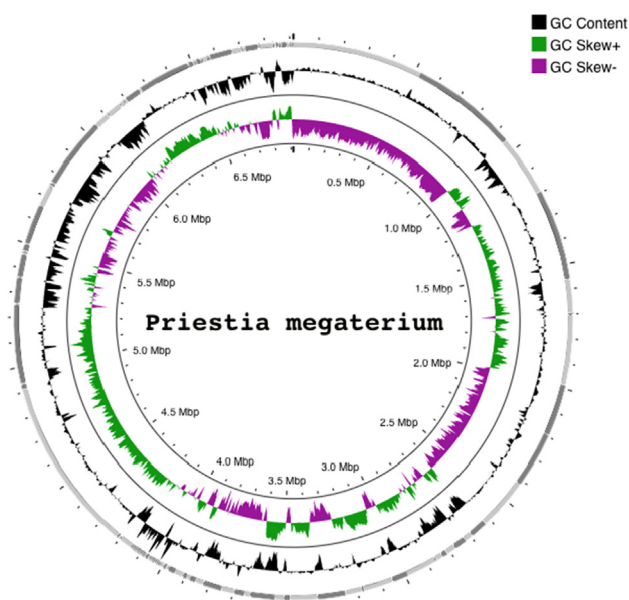


Fig. 2. Graphical circular map of the *P. megaterium* genome representing relevant genome features. The figure was built using CG viewer server (Grant and Stothard, 2008) software.

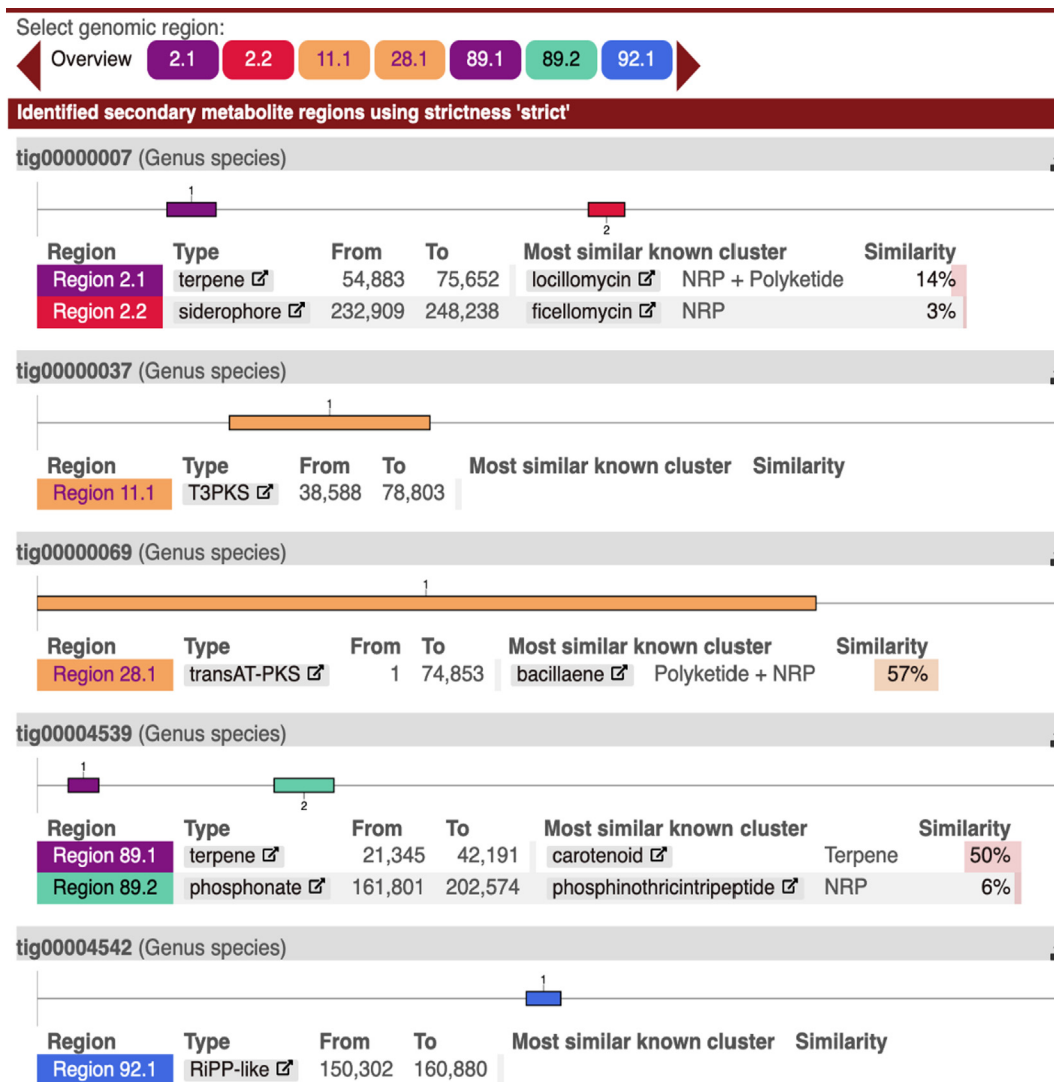


Fig. 3. Identification of a diverse set of biosynthetic gene clusters in the whole genomes of *P. megaterium*. Each cluster has its own putative secondary metabolites.

Table 3

The percentage similarity found in the correlated organisms and the identified compound of known biosynthetic class(es) with activity.

Biosynthetic class (es)	Compound	Compound activity	Homology	Correlated organism	Reference
Polyketide + NRP	Bacillaene	Antibiotic	57%	<i>B.velezensis</i> FZB42	(Moldenhauer et al., 2007)
Terpene	Carotenoid	Antioxidants	50%	<i>Halobacillus halophilus</i> DSM 2266	(Köcher et al., 2009)
Polyketide + NRP	Locillomycin Locillomycin B Locillomycin C	Antibacterial activity	14%	<i>B. subtilis</i>	(Luo et al., 2015, Luo et al., 2019)
NRP	Phosphinothricin-tripeptide	Herbicidal activity	6%	<i>S. viridochromogenes</i>	(Schwartz et al., 2004, Schwartz et al., 2005)
NRP	Ficellomycin	Antibiotic	3%	<i>S. ficellus</i>	(Liu et al., 2017)

the concentration of AuNPs was calculated to be 8.45 nM, where the extension coefficient (e) of $1.12 \times 10^8 \text{ cm}^{-1} \text{ M}^{-1}$ was used for 10 nm AuNPs (Mayer et al., 2003).

3.5. Intervention of *P. megaterium* cultivation medium with AuNPs and analytical profile of the crude extract

In the proposed research, we sought to investigate whether AuNPs could modulate secondary metabolite production in the

fresh environmental bacterial isolate. Our goal here was to identify the secondary metabolites that exhibited a correlation with AuNPs intervention. Briefly, the identified bacterial isolate (*P. megaterium*) was grown and seeded on certain nutrients. Then, a production medium was made with seeded bacteria and AuNPs were added. The production medium containing seeded bacteria without AuNPs was used as a control. After the incubation period was over, the cells were removed by centrifugation, and the supernatant was extracted with ethyl acetate. The extraction solvent was

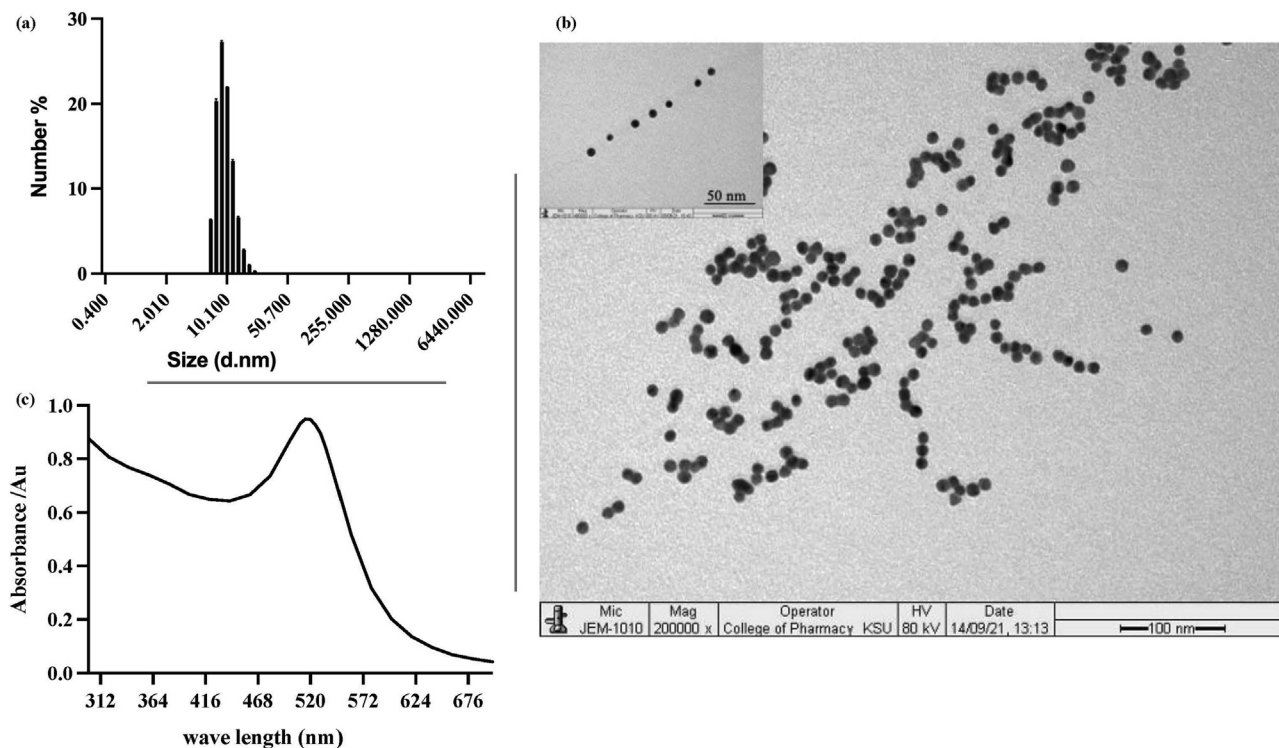


Fig. 4. Characterization of size and morphology of citrate-AuNPs using (a) DLS analysis, (b) TEM analysis, and (c) UV spectrophotometry of citrate-AuNPs solution.

evaporated, affording a sticky yellowish-brown crude extract with a total yield of 385 mg that was examined using different analytical techniques.

It has been postulated that due to their small size and spherical shape, silver nanoparticles (AgNPs) have the ability to penetrate bacterial cells (Raza et al., 2016). No studies have been reported on the AuNPs effect on the bacterial cell penetration or the secondary metabolites manipulation. However, a better understanding is needed of the AuNPs intervention with microbial metabolism. Therefore, we investigated to supplement the cultivation medium of *P. megaterium* with serial concentrations of citrate-AuNPs. Briefly, a seed culture of the isolated *P. megaterium* was prepared and inoculated with the same production media for all the samples. The samples were then exposed to different concentrations of 10 nm AuNPs (0, 25, 50, 250, 500, 1000, 1500, 2000 pM) and co-cultivated for six days. After the incubation period, the production media was centrifuged to remove the bacterial cells and AuNPs. The supernatant was extracted three times with ethyl acetate of equal volume, and the organic layers were combined and evaporated to afford the crude extract (Dimkić et al., 2013, Rajan and Kannabiran 2014). Then, the crude extracts were dissolved in 200 μ L of MeOH, filtered by 0.2 μ m PES syringe filters and analyzed using HPLC chromatography. The HPLC analysis was carried out using different conditions and optimized for chromatographic separation. As shown in Fig. 5, the extracted crude showed a dramatic difference with the presence of AuNPs in production media, where the intensity of two peaks (noted as 1 and 2 at the retention time of 5.6 and 5.3 min, respectively) increased with the rising concentration of AuNPs. The most significant change for the two peaks was observed at a concentration of 1000 pM AuNPs and, in comparison to the control, the intensity increased by 4.5- and 2.5-fold, respectively. Further increase of AuNPs concentration to 2000 pM only led to 2.8- and 1.2-fold change of the intensity of peaks 1 and 2, respectively.

We further dried and weighed the crude extracts corresponding to the different AuNPs concentrations added (Table 4). The results are in agreement with the HPLC analysis, where the gradually rising concentrations of AuNPs were accompanied by an increase in the yield of crude extracts. A maximum yield of 23 mg was achieved when 1000 pM of AuNPs was added, and this amount was 2 times higher than that from the control. When AuNPs concentration increased to 2000 pM, the yield was reduced to almost half of the maximum. This may be due to the fact that high concentrations of AuNPs could produce toxicity in *P. megaterium*. The toxicity of NPs to microorganisms is proportional to the dosage of nanomaterials and environmental variables, as well (Wu et al., 2020). Several studies have demonstrated that high concentrations of TiO₂ and CuO NPs could compromise the integrity of microbial cell membrane due to excessive Reactive oxygen species (ROS) production (Kumar et al., 2011, Liu et al., 2018). So far, there have been no reports of microbial toxicity induced by AuNPs and much attention has been given to their toxicity on human cells. Some findings had attributed the toxicity of AuNPs to the use of very high concentrations and different cell type sensitivities (Falagan-Lotsch et al., 2016).

3.6. Metabolite profiling using genome mining

Genome mining utilizes modern bioinformatics to recognize specific functional genes or gene clusters from genome sequences. With the rapid development of gene sequencing and the decrease of sequencing cost, microbial genome could be readily determined, making genome mining an efficient strategy to find new metabolites. The antibiotics and secondary metabolite analysis shell (AntiSMASH) is one of the most commonly used genome mining tools that have been used to identify wide genome, annotate and analyze secondary metabolite biosynthetic gene clusters, and help to estimate the types of compounds encoded by the gene clusters.

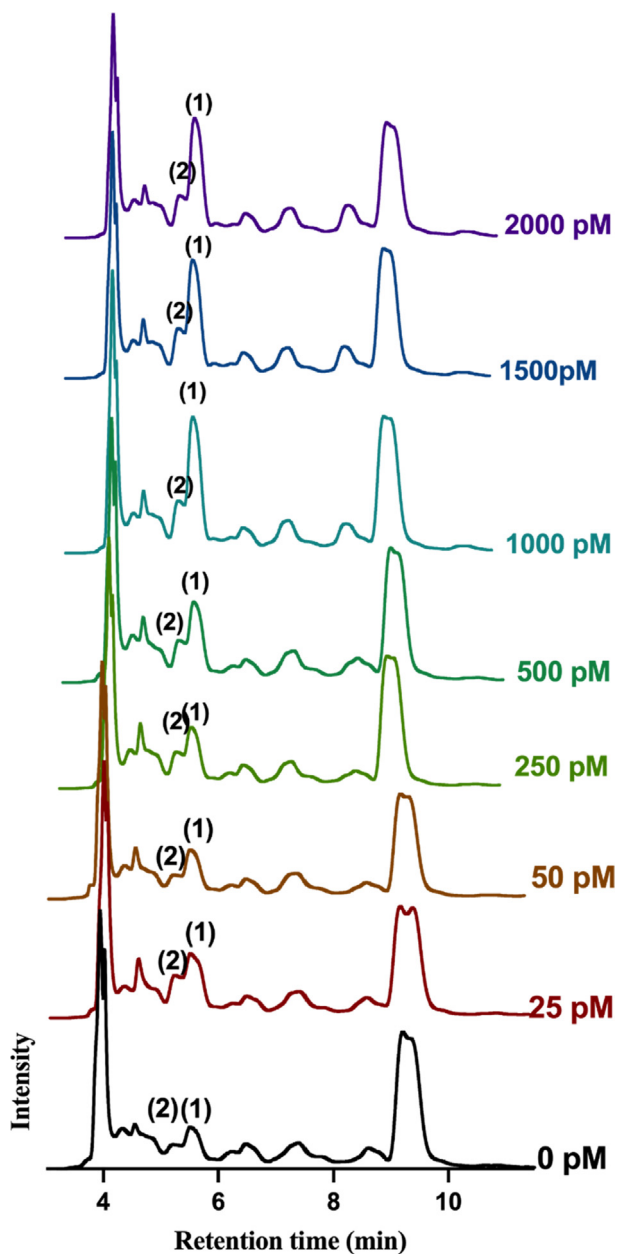


Fig. 5. HPLC analysis of the crude extract from microbial media upon exposure to varied concentrations of AuNPs (0 pM is the control as no AuNPs had been added).

Table 4
The mass yield of crude extracts when dried.

Concentration of AuNPs, pM	weight of crude extract, mg
0	11.33
25	12
50	12.67
250	13
500	14
1000	23
1500	19.67
2000	12

In the past, thousands of BGCs from microbial genomes have been identified and curated in public databases such as Minimum Information about a Biosynthetic Gene Cluster (MIBiG) Repository. MIBiG specification provides a robust community standard for annotations and metadata on BGCs and their molecular products.

Fig. 6 demonstrates the MIBiG comparison of the molecules that have structural similarities with other organisms. Here, we only focused on terpenes, flavanone and alkaloids molecules such as squalestatin S1, eremophilene, chuangxinmycin, naringenin, and erdasporine A, erdasporine B, erdasporine C.

Interestingly, we have identified a putative cytochrome P450 *YjiB* protein encoded for gene *yjiB_1* (located from 72,891–74,105 of total 1215 nt.) that showed to be responsible for producing most of the compounds listed in Table 5.

Seven BGCs were extracted from the *P. megaterium* genomic draft based on AntiSMASH analysis as seen in Fig. 3. Among them, terpene cluster suggests different molecules as appeared in MIBiG comparison that shares structural similarities with other organisms as seen in Fig. 6 and Table 5. Mainly, the second molecule named naringenin with reference BGC0001310.1 has been found in *S. clavuligerus*. The Geneious software was used to show the genomic annotation of *S. clavuligerus* (Fig. 7), and Terpene/ T3PKS clusters were found to be present in *S. clavuligerus* genomic annotation. Chalcone synthase (CHS) and cytochrome P450 proteins have been previously identified to be responsible for the biosynthesis of a naringenin metabolite in *Streptomyces* (Álvarez-Álvarez et al., 2015).

It has been demonstrated that the *yjiB* protein found in the bacterial isolate genomic draft is responsible for the production of a variety of secondary metabolites. We investigated the sequence alignments of both cytochrome P450 proteins that exist in *S. clavuligerus* encode for (NcyP), as well as the other putative cytochrome P450 protein that originates from our bacterial isolate (*yjiB*). The alignments were achieved using Geneious software. Both sequences had a length (mean) of 1,290 bp, and the percentage of pairwise identity was recorded by 47.3%. Then, we further investigated the T3PKS cluster by looking for CHS similarity and discovered that the percentage of pairwise identity was 48.1%. This led us to conclude that the T3PKS cluster is quite comparable to those found in *S. clavuligerus*. This provides evidence of the notion that *P. megaterium* has a particular CHS enzyme, which is the key enzyme that controls the production of naringenin-related compounds.

The crude extract before and after AuNPs intervention was subjected to fractionation using silica gel column chromatography to obtain the two major fractions that appeared in HPLC analysis noted as 1 and 2 (Fig. 5). When subjected to ESI-MS/MS analysis, the masses of fractions 1 and 2 were confirmed to be 254 and 270 Da, respectively (Fig. 8). The parent peak of fraction 1 showed protonated molecular ions at *m/z* 255 and fragmentations at *m/z* 227, 199, 181, 153, 137, and 128. For fraction 2, the parent peak showed protonate molecular ions at 271 and fragment ions at 215, 168, 153, and 115. Both fractions carry the same fragmentation ion *m/z* 153, which could indicate sharing the core of the naringenin chalcone (Fig. 9) (Xu et al., 2009). This is in line with previous genome mining results that had identified a putative BGC that produces naringenin derivatives.

There has never been a reported study of naringenin-related compounds production and isolation in *P. megaterium*. Therefore, it would be worthwhile investigating whether the naringenin molecule and putative gene clusters in *P. megaterium* are comparable to those found in *S. clavuligerus* and/ or whether the production

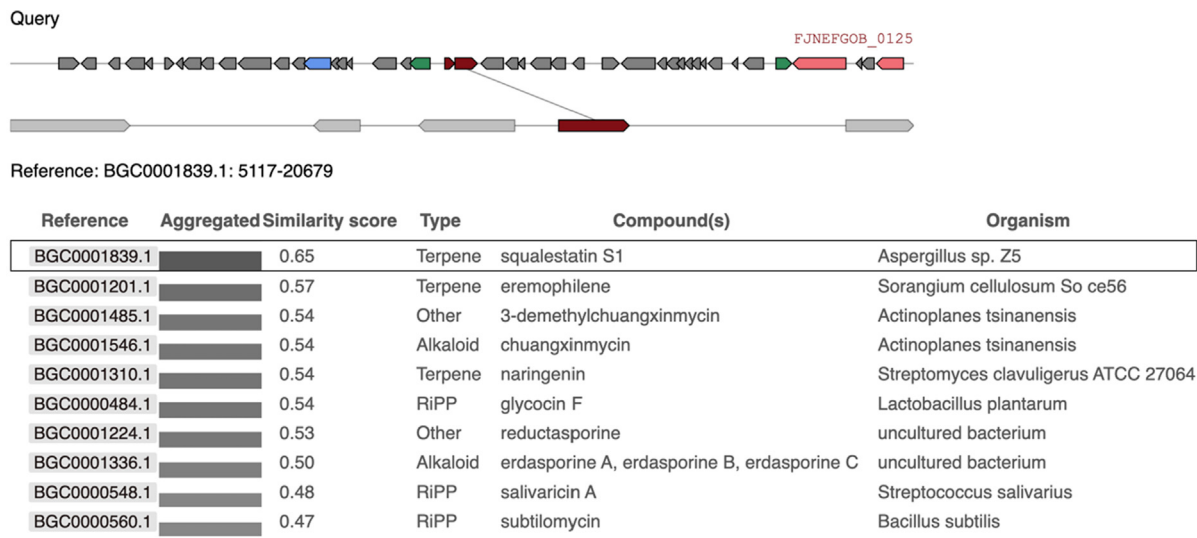


Fig. 6. List of different classes of compounds from the Terpene cluster that can share similarities with other organisms.

Table 5

The compound and their structure of the metabolites produced by yjiB protein and related origin of microorganisms.

Compound/ Type	Structure	Molecular weight	Related organisms	Reference
Eremophilene/ sesquiterpene		204.35	<i>Sorangium cellulosum</i> So ce56	(Schiffrin et al., 2015)
Naringenin/ flavanone		272.25	<i>S. clavuligerus</i>	(Álvarez-Álvarez et al., 2015)
3-demethylchuangxinmycin/ alkaloid		219.26	<i>Actinoplanes tsinanensis</i>	(Zuo et al., 2016)
Chuangxinmycin/ alkaloid		233.29	<i>Actinoplanes tsinanensis</i>	(Xu et al., 2018)
Reductasporine/ alkaloid		326.17	uncultured bacterium	(Chang et al., 2015)
Erdasporine A/ alkaloid		369.4	uncultured bacterium	(Chang et al., 2013)

(continued on next page)

Table 5 (continued)

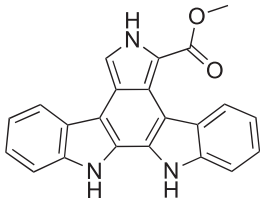
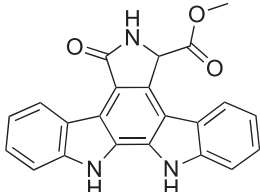
Compound/Type	Structure	Molecular weight	Related organisms	Reference
Erdasporine B/ alkaloid		353.4		
erdasporine C/ alkaloid		369.4		



Fig. 7. *S. clavuligerus* accession# BGC0001310 genome sequence annotation display both clusters of Terpene in red and T3PKS that hold cytochrome P450 protein in green. This annotation extracted from Geneious version 2022.2 created by Biomatters. Available from <https://www.geneious.com>.

of isoflavone or flavones metabolites is affected by AuNPs intervention.

4. Conclusion

We used the gDNA sequencing to complete a comprehensive genomic investigation of an unknown isolated strain from potato crops. This contributed to the identification of compounds involved

in various BGCs and the prediction of natural product structures. Our bioinformatic findings showed that the isolated strain is a member of the species, *Priestia megaterium* and possesses seven BGCs, including the most crucial cluster T3PKS. These bioinformatic observations help to further isolate and identify secondary metabolites predicted in *P. megaterium*. We also investigated the effect of various concentrations and analyzed the metabolic profile influence of AuNPs on *P. megaterium* culture. This study revealed the potential to increase the biosynthesis of secondary metabolites in a new *P. megaterium* environmental isolate using AuNPs intervention. The two crucial compounds have been enhanced significantly as approved by using HPLC–PDA. This application generally yielded better results in terms of yield parameters compared to the control. Our research can provide some new insights about the effects of AuNPs on the genetic manipulation for the production of secondary metabolism. The studied technique could be promising for prospective research on nano-biotechnology and drug discovery of new natural products.

Author contributions

The manuscript was written through contributions of all authors. All authors have given approval to the final version of the manuscript. HA designed the research plan. NA performed the experiments. HA, ML, and NA analyzed the data and wrote the manuscript.

Funding

This work was supported the Researchers Supporting Project, King Saud University, Riyadh, Saudi Arabia for funding this work through grant no. RSPD2023R566.

Declaration of Competing Interest

The authors declare that they have no known competing financial interests or personal relationships that could have appeared to influence the work reported in this paper.

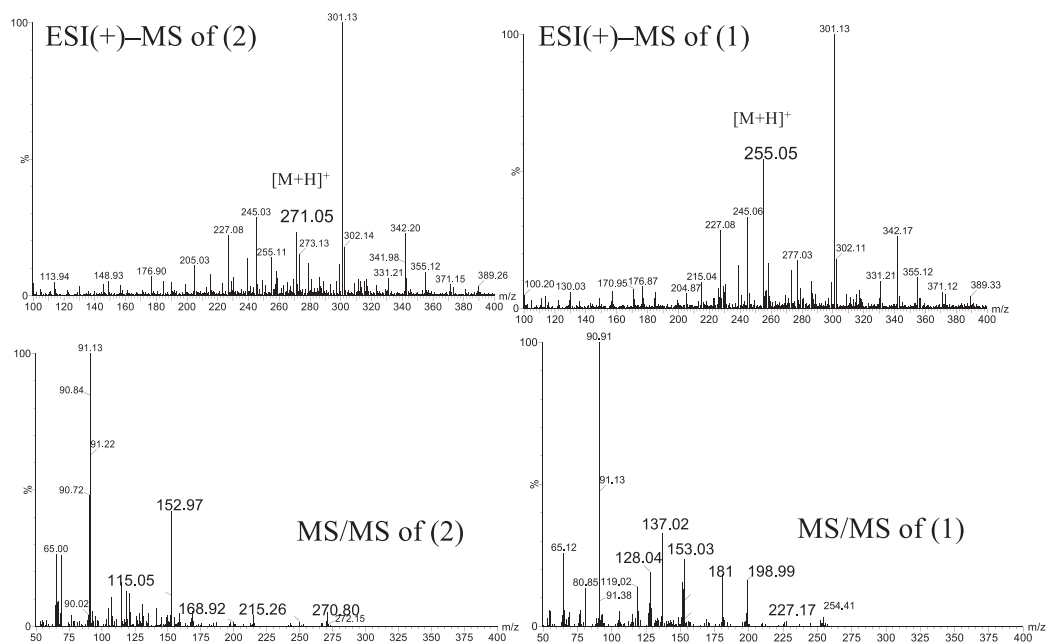
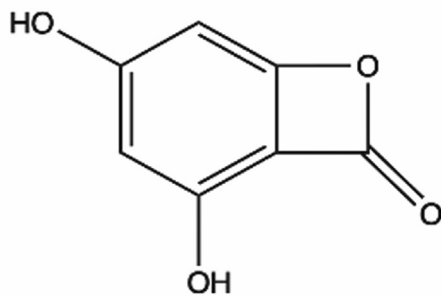
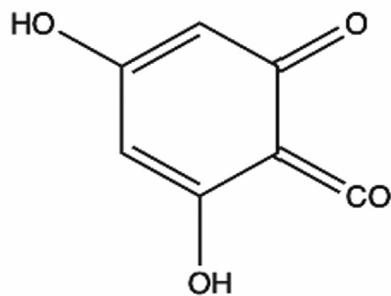


Fig. 8. Comparison of the parent's ions obtained in ESI-MS/MS experiments of protonated compounds 1 and 2.

Chemical Formula: $C_7H_4O_4$
Exact Mass: 152.01



Chemical Formula: $C_7H_4O_4$
Exact Mass: 152.01

Fig. 9. Fragment of naringenin chalcone (m/z 153).

Acknowledgments

The authors extend their appreciation to the Researchers Supporting Project, King Saud University, Riyadh, Saudi Arabia for funding this work through grant no. RSPD2023R566

Appendix A. Supplementary data

Supplementary data to this article can be found online at <https://doi.org/10.1016/j.jpsp.2023.04.016>.

References

- Abdelhameed, A.S., Attwa, M.W., Kadi, A.A., 2020. Identification of iminium intermediates generation in the metabolism of tepotinib using LC-MS/MS: in silico and practical approaches to bioactivation pathway elucidation. *Molecules* 25, 5004. <https://doi.org/10.3390/molecules25215004>.
- Alkotaini, B., Sathiyamoorthi, E., Kim, B.S., 2015. Potential of *Bacillus megaterium* for production of polyhydroxyalkanoates using the red alga *Gelidium amansii*. *Biotechnology and bioengineering*. 20, 856–860.
- Álvarez-Álvarez, R., Botas, A., Albillos, S.M., et al., 2015. Molecular genetics of naringenin biosynthesis, a typical plant secondary metabolite produced by *Streptomyces clavuligerus*. *Microb Cell Fact.* 14, 1–12. <https://doi.org/10.1186/s12934-015-0373-7>.
- Antoraz, S., Santamaría, R.I., Díaz, M., et al., 2015. Toward a new focus in antibiotic and drug discovery from the *Streptomyces* arsenal. *Front. Microbiol.* 6, 461. <https://doi.org/10.3389/fmicb.2015.00461>.
- Biedendieck, R., Knuuti, T., Moore, S.J., et al., 2021. The “beauty in the beast”—the multiple uses of *Priestia megaterium* in biotechnology. *Appl. Microbiol. Biotechnol.* 105, 5719–5737.
- Blin, K., Shaw, S., Steinke, K., et al., 2019. antiSMASH 5.0: updates to the secondary metabolite genome mining pipeline. *Nucleic Acids Res.* 47, W81–W87.
- Brzonkalik, K., Hümmel, D., Syltatk, C., et al., 2012. Influence of pH and carbon to nitrogen ratio on mycotoxin production by *Alternaria alternata* in submerged cultivation. *AMB Express* 2, 1–8. <https://doi.org/10.1186/2191-0855-2-28>.
- Chang, F.-Y., Ternei, M.A., Calle, P.Y., et al., 2013. Discovery and synthetic refactoring of tryptophan dimer gene clusters from the environment. *J. Am. Chem. Soc.* 135, 17906–17912. <https://doi.org/10.1021/ja408683p>.
- Chang, F.-Y., Ternei, M.A., Calle, P.Y., et al., 2015. Targeted metagenomics: Finding rare tryptophan dimer natural products in the environment. *J. Am. Chem. Soc.* 137, 6044–6052. <https://doi.org/10.1021/jacs.5b01968>.
- Coltin, J., Corroler, D., Lemoine, M., et al., 2022. Mineral medium design based on macro and trace element requirements for high cell density cultures of *Priestia megaterium* DSM 509. *Biochem. Eng. J.* 187, 108625.

- Cui, L., Yang, C., Wang, Y., et al., 2021. Potential of an endophytic bacteria *Bacillus amyloliquefaciens* 3–5 as biocontrol agent against potato scab. *Microb. Pathog.* 105382.
- Dimkić, I., Živković, S., Berić, T., et al., 2013. Characterization and evaluation of two *Bacillus* strains, SS-12.6 and SS-13.1, as potential agents for the control of phytopathogenic bacteria and fungi. *Biol. Control.* 65, 312–321. <https://doi.org/10.1016/j.biocontrol.2013.03.012>.
- Falagan-Lotsch, P., Grzincic, E.M., Murphy, C.J., 2016. One low-dose exposure of gold nanoparticles induces long-term changes in human cells. *Proc. Natl. Acad. Sci.* 113, 13318–13323.
- Fekete, T., 2005. *Bacillus* species and related genera other than *Bacillus anthracis*. Mandell, Douglas, and Bennett's principles and practice of infectious diseases., 2493–2496.
- Grasso, G., Zane, D., Dragone, R., 2019. Microbial nanotechnology: challenges and prospects for green biocatalytic synthesis of nanoscale materials for sensoristic and biomedical applications. *Nanomaterials* 10, 11.
- Gupta, R.S., Patel, S., Saini, N., et al., 2020. Robust demarcation of 17 distinct *Bacillus* species clades, proposed as novel Bacillaceae genera, by phylogenomics and comparative genomic analyses: description of *Robertmurraya kyonggiensis* sp. nov. and proposal for an emended genus *Bacillus* limiting it only to the members of the *Subtilis* and *Cereus* clades of species. *Int. J. Syst. Evol. Microbiol.* 70, 5753–5798.
- Han, J., Cheng, J., Yoon, T., et al., 2005. Biological control agent of common scab disease by antagonistic strain *Bacillus* sp. sunhua. *J. Appl. Microbiol.* 99, 213–221.
- Hoomstra, D., Andersson, M.A., Teplova, V.V., et al., 2013. Potato crop as a source of emetic *Bacillus cereus* and cereulide-induced mammalian cell toxicity. *Appl. Environ. Microbiol.* 79, 3534–3543.
- Kai, M., 2020. Diversity and distribution of volatile secondary metabolites throughout *Bacillus subtilis* isolates. *Front. Microbiol.* 11, 559.
- Kautsar, S.A., Bliin, K., Shaw, S., et al., 2020. MIBiG 2.0: a repository for biosynthetic gene clusters of known function. *Nucleic Acids Res.* 48, D454–D458.
- Kenshole, E., Herisse, M., Michael, M., et al., 2021. Natural product discovery through microbial genome mining. *Curr. Opin. Chem. Biol.* 60, 47–54.
- Khedher, S.B., Kilani-Feki, O., Dammak, M., et al., 2015. Efficacy of *Bacillus subtilis* V26 as a biological control agent against *Rhizoctonia solani* on potato. *C. R. Biol.* 338, 784–792.
- Köcher, S., Breitenbach, J., Müller, V., et al., 2009. Structure, function and biosynthesis of carotenoids in the moderately halophilic bacterium *Halobacillus halophilus*. *Arch. Microbiol.* 191, 95–104. <https://doi.org/10.1007/s00203-008-0431-1>.
- Koren, S., Walenz, B.P., Berlin, K., et al., 2017. Canu: scalable and accurate long-read assembly via adaptive k-mer weighting and repeat separation. *Genome Res.* 27, 722–736 <https://doi.org/10.1101/gr.215087.116>.
- Kumar, A., Pandey, A.K., Singh, S.S., et al., 2011. Engineered ZnO and TiO₂ nanoparticles induce oxidative stress and DNA damage leading to reduced viability of *Escherichia coli*. *Free Radic. Biol. Med.* 51, 1872–1881. <https://doi.org/10.1016/j.freeradbiomed.2011.08.025>.
- Kumar, A., Asthana, M., Gupta, A., et al., 2018. Secondary metabolism and antimicrobial metabolites of *Penicillium*. *New and Future Developments in Microbial. Biotechnol. Bioeng. Elsevier*, 47–68.
- Lambert, D., Loria, R., Labeda, D., et al., 2007. Recommendation for the conservation of the name *Streptomyces scabies*. Request for an Opinion. *Int. J. Syst. Evol. Microbiol.* 57, 2447–2448.
- Liang, M., Lin, I.-C., Whittaker, M.R., et al., 2010. Cellular uptake of densely packed polymer coatings on gold nanoparticles. *ACS Nano* 4, 403–413. <https://doi.org/10.1021/nn9011237>.
- Liu, Y., Li, M., Mu, H., et al., 2017. Identification and characterization of the ficellomycin biosynthesis gene cluster from *Streptomyces ficellus*. *Appl. Microbiol. Biotechnol.* 101, 7589–7602. <https://doi.org/10.1007/s00253-017-8465-4>.
- Liu, X., Tang, J., Wang, L., et al., 2018. Mechanisms of oxidative stress caused by CuO nanoparticles to membranes of the bacterium *Streptomyces coelicolor* M145. *Ecotoxicol. Environ. Saf.* 158, 123–130. <https://doi.org/10.1016/j.ecoenv.2018.04.007>.
- Liu, X., Tang, J., Wang, L., et al., 2019. Mechanism of CuO nano-particles on stimulating production of actinorhodin in *Streptomyces coelicolor* by transcriptional analysis. *Sci. Rep.* 9, 1–10.
- Loria, R., Kers, J., Joshi, M., 2006. Evolution of plant pathogenicity in *Streptomyces*. *Annu. Rev. Phytopathol.* 44, 469–487.
- Luo, C., Liu, X., Zhou, H., et al., 2015. Nonribosomal peptide synthase gene clusters for lipopeptide biosynthesis in *Bacillus subtilis* 916 and their phenotypic functions. *Appl. Environ. Microbiol.* 81, 422–431. <https://doi.org/10.1128/AEM.02921-14>.
- Luo, C., Chen, Y., Liu, X., et al., 2019. Engineered biosynthesis of cyclic lipopeptide locillomycins in surrogate host *Bacillus velezensis* FZB42 and derivative strains enhance antibacterial activity. *Appl. Microbiol. Biotechnol.* 103, 4467–4481. <https://doi.org/10.1007/s00253-019-09784-1>.
- Mandal, D. and A. Basu, 2021. Role of Heavy-Metal Resistant Bacteria Isolated from Rhizosphere in Bioremediation and Plant Development. *Rhizobiology: Molecular Physiology of Plant Roots*, Springer: 411–435.
- Marslin, G., Sheeba, C.J., Franklin, G., 2017. Nanoparticles alter secondary metabolism in plants via ROS burst. *Front. Plant Sci.* 8, 832. <https://doi.org/10.3389/fpls.2017.00832>.
- Maye, M.M., Han, L., Kariuki, N.N., et al., 2003. Gold and alloy nanoparticles in solution and thin film assembly: spectrophotometric determination of molar absorptivity. *Anal. Chim. Acta* 496, 17–27.
- Moat, A.G., Foster, J.W., Spector, M.P., 2002. *Microbial physiology*. John Wiley & Sons.
- Moldenhauer, J., Chen, X.H., Borriss, R., et al., 2007. Biosynthesis of the antibiotic bacillaene, the product of a giant polyketide synthase complex of the trans-AT family. *Angew. Chem. Int. Ed. Engl.* 46, 8195–8197. <https://doi.org/10.1002/anie.200703386>.
- Nadaf, N.Y., Kanase, S.S., 2019. Biosynthesis of gold nanoparticles by *Bacillus marisflavi* and its potential in catalytic dye degradation. *Arab. J. Chem.* 12, 4806–4814.
- Pinjari, A.B., Bramhachari, P.V., 2018. Detection and Expression of Biosynthetic Gene Clusters in Actinobacteria. *New and Future Developments in Microbial. Biotechnol. Bioeng. Elsevier*, 245–255.
- Rajan, B.M., Kannabiran, K., 2014. Extraction and identification of antibacterial secondary metabolites from marine *Streptomyces* sp. VITBRK2. *Int. J. Mol. Cell Med.* 3, 130.
- Raza, M.A., Kanwal, Z., Rauf, A., et al., 2016. Size-and shape-dependent antibacterial studies of silver nanoparticles synthesized by wet chemical routes. *Nanomaterials* 6, 74.
- Ren, H., Shi, C., Zhao, H., 2020. Computational tools for discovering and engineering natural product biosynthetic pathways. *Iscience.* 23. <https://doi.org/10.1016/j.isci.2019.100795>.
- Ruiz, B., Chávez, A., Forero, A., et al., 2010. Production of microbial secondary metabolites: regulation by the carbon source. *Crit. Rev. Microbiol.* 36, 146–167. <https://doi.org/10.3109/10408410903489576>.
- Sandle, T., 2004. Gram's stain: history and explanation of the fundamental technique of determinative bacteriology. *IST Science and Technology.* 54, 3–4.
- Schiffrin, A., Ly, T.T., Günnewich, N., et al., 2015. Characterization of the Gene Cluster CYP264B1-geoA from *Sorangium cellulosum* So ce56: Biosynthesis of (+)-Eremophilene and Its Hydroxylation. *Chembiochem* 16, 337–344. <https://doi.org/10.1002/cbic.201402443>.
- Schwartz, D., Berger, S., Heinzelmann, E., et al., 2004. Biosynthetic gene cluster of the herbicide phosphinothricin tripeptide from *Streptomyces viridochromogenes* Tu494. *Appl. Environ. Microbiol.* 70, 7093–7102. <https://doi.org/10.1128/AEM.70.12.7093-7102.2004>.
- Schwartz, D., Grammel, N., Heinzelmann, E., et al., 2005. Phosphinothricin tripeptide synthetases in *Streptomyces viridochromogenes* Tu494. *Antimicrob. Agents Chemother.* 49, 4598–4607. <https://doi.org/10.1128/AAC.49.11.4598-4607.2005>.
- Seemann, T., 2014. Prokka: rapid prokaryotic genome annotation. *Bioinformatics* 30, 2068–2069.
- Shahid, S., Mosrati, R., Ledauphin, J., et al., 2013. Impact of carbon source and variable nitrogen conditions on bacterial biosynthesis of polyhydroxyalkanoates: evidence of an atypical metabolism in *Bacillus megaterium* DSM 509. *J. Biosci. Bioeng.* 116, 302–308.
- Singh, S., Vidyarthi, A.S., Nigam, V.K., et al., 2014. Extracellular facile biosynthesis, characterization and stability of gold nanoparticles by *Bacillus licheniformis*. *Artif. Cells Nanomed. Biotechnol.* 42, 6–12.
- Srinath, B., Namratha, K., Byrappa, K., 2018. Eco-friendly synthesis of gold nanoparticles by *Bacillus subtilis* and their environmental applications. *Adv. Sci. Lett.* 24, 5942–5946.
- Stothard, P., Wishart, D.S., 2005. Circular genome visualization and exploration using CGView. *Bioinformatics* 21, 537–539.
- Suhandono, S., Kusumawardhani, M.K., Aditiawati, P., 2016. Isolation and molecular identification of endophytic bacteria from Rambutan fruits (*Nephelium lappaceum* L.) cultivar Binjai. *HAYATI Journal of Biosciences.* 23, 39–44.
- Tanizawa, Y., Fujisawa, T., Nakamura, Y., 2017. DFAST: a flexible prokaryotic genome annotation pipeline for faster genome publication. *Bioinformatics* 34, 1037–1039. <https://doi.org/10.1093/bioinformatics/btx713>.
- van Der Hoof, J.J., Mohimani, H., Bauermeister, A., et al., 2020. Linking genomics and metabolomics to chart specialized metabolic diversity. *Chem. Soc. Rev.* 49, 3297–3314.
- Wang, B., Guo, F., Dong, S.-H., et al., 2019. Activation of silent biosynthetic gene clusters using transcription factor decoys. *Nat. Chem. Biol.* 15, 111–114. <https://doi.org/10.1038/s41589-018-0187-0>.
- Wu, Y., Rong, X., Zhang, C., et al., 2020. Response of the intertidal microbial community structure and metabolic profiles to zinc oxide nanoparticle exposure. *Int. J. Environ. Res. Public Health* 17, 2253.
- Xie, Y., Peng, Q., Ji, Y., et al., 2021. Isolation and identification of antibacterial bioactive compounds from *Bacillus megaterium* L2. *Front. Microbiol.* 12.
- Xu, F., Liu, Y., Zhang, Z., et al., 2009. Quasi-MSn identification of flavanone 7-glycoside isomers in Da Chengqi Tang by high performance liquid chromatography-tandem mass spectrometry. *Chin. Med.* 4, 1–10.
- Xu, X., Zhou, H., Liu, Y., et al., 2018. Heterologous expression guides identification of the biosynthetic gene cluster of chuangxinmycin, an indole alkaloid antibiotic. *J. Nat. Prod.* 81, 1060–1064. <https://doi.org/10.1021/acs.jnatprod.7b00835>.
- Zong, G., Fu, J., Zhang, P., et al., 2021. Use of elicitors to enhance or activate the antibiotic production in *Streptomyces*. *Crit. Rev. Biotechnol.* 1–24.
- Zuo, L., Zhao, W., Jiang, Z., et al., 2016. Identification of 3-demethylchuangxinmycin from *Actinoplanes tsinanensis* CICC 200056. *Yao Xue Xue Bao* 51, 105–109.